OPEN

Emissions of methane from offshore oil and gas platforms in Southeast Asia

Hideki Nara, Hiroshi Tanimoto, Yasunori Tohjima, Hitoshi Mukai, Yukihiro Nojiri & Toshinobu Machida

Center for Global Environmental Research, National Institute for Environmental Studies, 16-2 Onogawa, Tsukuba, Ibaraki 305-8506, Japan.

Methane is a substantial contributor to climate change. It also contributes to maintaining the background levels of tropospheric ozone. Among a variety of CH_4 sources, current estimates suggest that CH_4 emissions from oil and gas processes account for approximately 20% of worldwide anthropogenic emissions. Here, we report on observational evidence of CH_4 emissions from offshore oil and gas platforms in Southeast Asia, detected by a highly time-resolved spectroscopic monitoring technique deployed onboard cargo ships of opportunity. We often encountered CH_4 plumes originating from operational flaring/venting and fugitive emissions off the coast of the Malay Peninsula and Borneo. Using night-light imagery from satellites, we discovered more offshore platforms in this region than are accounted for in the emission inventory. Our results demonstrate that current knowledge regarding CH_4 emissions from offshore platforms in Southeast Asia has considerable uncertainty and therefore, emission inventories used for modeling and assessment need to be re-examined.

Atmospheric CH_4 is an important component of short-lived climate pollutants that contribute both directly and indirectly to radiative forcing. It is also known that CH_4 contributes to maintaining the background levels of tropospheric ozone[1]. CH_4 is emitted from a variety of natural (e.g., wetlands, oceans, termites, and clathrates) and anthropogenic (e.g., fossil-fuel exploitation, ruminant animals, rice cultivation, waste management, and biomass burning) sources. Because of the shorter atmospheric lifetime (about nine years[2]) of CH_4 than CO_2, a reduction of anthropogenic emissions of CH_4 would be an effective means of abating global warming in the near future[3,4]. However, to establish strategies for the mitigation of global warming, a quantitative understanding of the global CH_4 budget is required.

Atmospheric abundance of CH_4 has been increasing from pre-industrial levels of about 700 nmol mol^{-1} (hereafter referred to as ppb) with large year-to-year fluctuations in its growth rate[5]. Among the many studies that have investigated the distribution and temporal variation of CH_4, several have reported conflicting results[6–9]. Some recent studies have suggested the existence of previously unrecognized sources of CH_4. For example, satellite observations have been combined with inverse modeling techniques using CH_4 retrievals from the Scanning Imaging Absorption Spectrometer for Atmospheric Chartography (SCIAMACHY) to provide a global distribution map of CH_4 that suggests there are many emission hot spots in areas where surface observations are scarce[10]. The first airborne in situ measurements of CH_4 over the Amazon region during the BARCA (Balanço Atmosphérico Regional de Carbono na Amazônia) campaign revealed strong CH_4 emissions from the Amazonian wetlands[11]. Regular aircraft observations from the CARIBIC (Civil Aircraft for the Regular Investigation of the atmosphere Based on an Instrument Container) program suggest strong biogenic emissions from India that cannot be attributed solely to rice cultivation[12]. These studies show that our current understanding regarding the sources of CH_4 emissions is inadequate and that greater effort is needed to obtain better knowledge both of the strength of CH_4 emissions and of the distribution of the sources. For this purpose, a more systematic approach is required regarding the acquisition of CH_4 observations in areas where observational data are sporadic or sparse.

Since 1992, the National Institute for Environmental Studies (NIES) has conducted a voluntary observing ships (VOS) program of long-term atmospheric monitoring of climatically important trace gases over the Pacific Ocean[13,14]. In the Southeast Asian region, atmospheric monitoring as part of the NIES-VOS program commenced in September 2007. Although flask sampling was initially used for CH_4 monitoring, since 2009, the program has been augmented by the use of continuous measurements that capture the highly variable features of CH_4 in the regionally polluted air in Southeast Asia. In this paper, we present the first results of the high-resolution continuous onboard measurements of CH_4 in the marine boundary layer (MBL) in the Southeast Asian region between September 2009 and April 2012. We focus on the CH_4 distribution in the northern equatorial region,
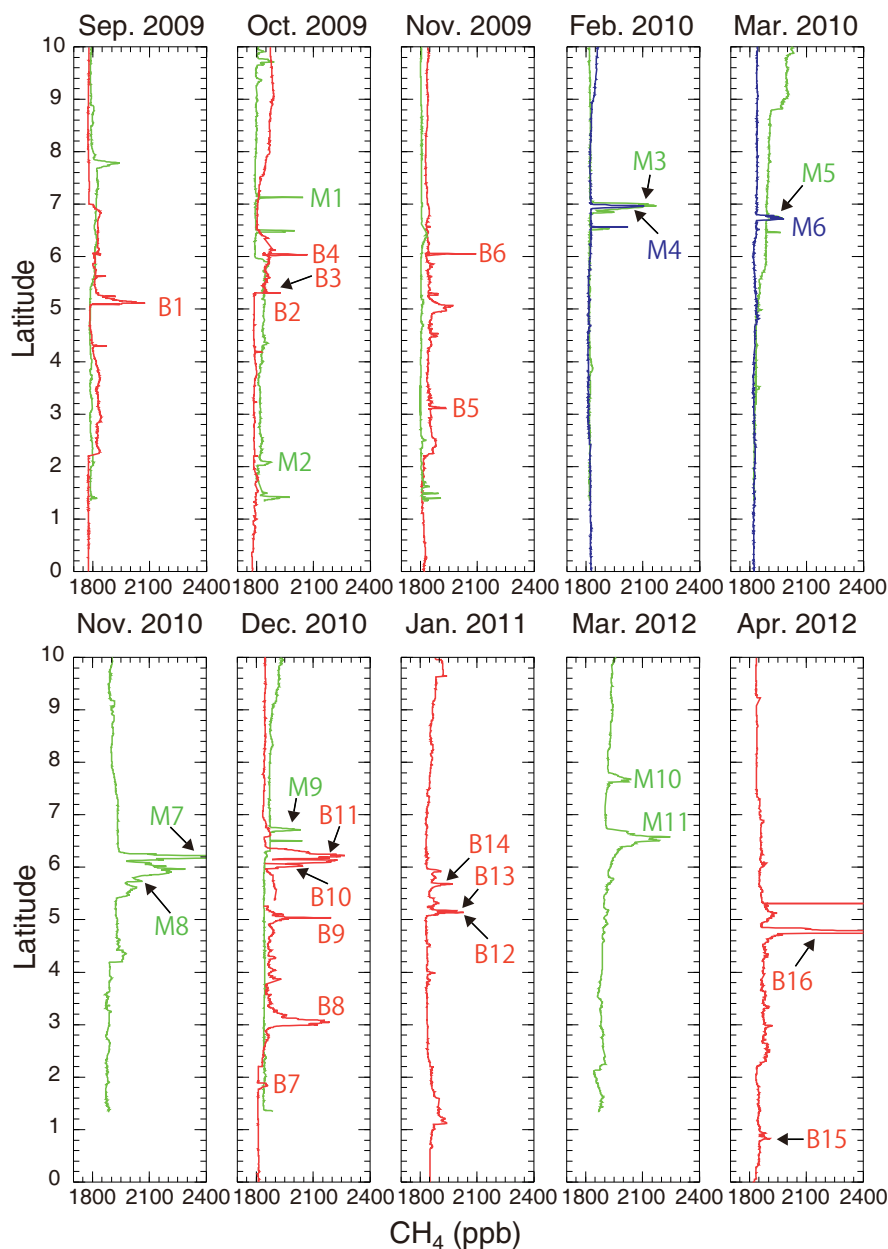
Figure 1 | Latitudinal distribution of 1-min temporally averaged CH$_4$ mole fractions between latitude 10°N and the equator observed during eight voyages along the Southeast Asian shipping routes between September 2009 and April 2012. Mole fractions of CH$_4$ are color coded according to the shipping routes: green for the southbound Asia route, blue for northbound Asia route, and red for northbound Borneo route. Peak numbers are allocated for only the Malay and Borneo peaks (preceded by M or B) that showed substantial CH$_4$ increase (>50 ppb) and positive correlation between CH$_4$ and CO$_2$ ($R > 0.4$, p-value < 0.05) and that had peak durations of more than 10 min.

where strong CH$_4$ peaks were observed off the east coast of the Malay Peninsula and the northwest coast of Borneo, and we examine the emission sources responsible for these observed CH$_4$ peaks.

Results

Although shipping operations were disrupted temporarily by the global financial crisis and the 2011 Great East Japan Earthquake, we were able to undertake observations during eight voyages between September 2009 and April 2012. Many CH$_4$ peaks were observed in the northern equatorial region along Southeast Asian routes (Figure 1); see Methods section for further details. The locations at which these peaks occurred were concentrated in two areas: off the east coast of the Malay Peninsula (39 peaks) and off the northwest coast of Borneo (55 peaks); they are referred to hereafter as the Malay

and Borneo peaks, respectively. The Malay peaks were observed largely between latitudes 8°N and 5.5°N along both the northbound and southbound routes, while the Borneo peaks were observed between latitudes 6.5°N and 4.5°N along the northbound Borneo route. Although the durations of all observed CH$_4$ peaks were short, between several minutes to one hour, the increases of the mole fraction of CH$_4$ were considerable, i.e., up to about 1100 ppb above the baseline levels for the Southeast Asian region. Concurrent with the CH$_4$ peaks, we observed simultaneous CO$_2$ peaks, and the positive correlation between these CO$_2$ and CH$_4$ mole fractions suggested a common local, non-biogenic emission source for these gases.

To identify sources of CH$_4$ emission, we examined satellite-observed night-light data from the US Air Force Defense Meteorological Satellite Project Operational Linescan System (DMSP/OLS),
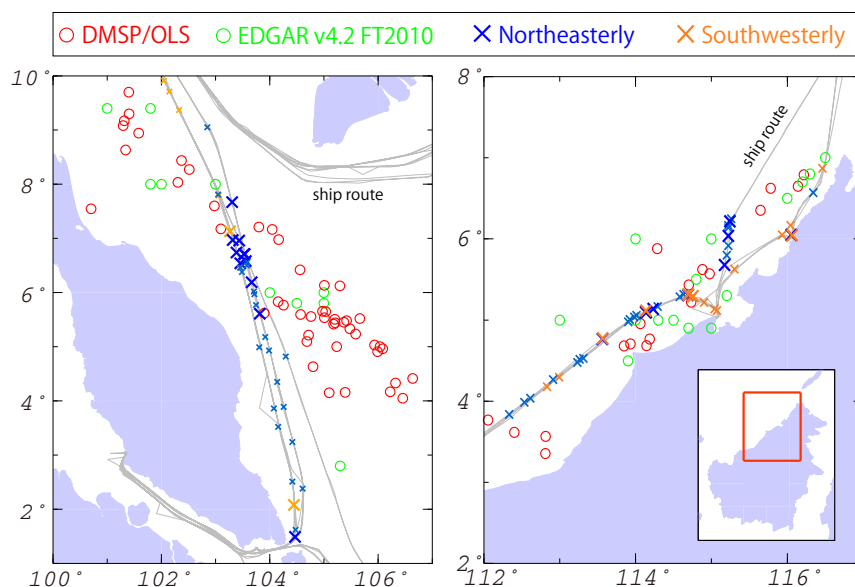
Figure 2 | Distribution of CH$_4$ peaks observed during this study and offshore platforms off the east coast of the Malay Peninsula (left) and the northwest coast of Borneo (right). Crosses are the locations where CH$_4$ peaks were observed and their colors explain wind patterns when each CH$_4$ peak was observed (blue: northeasterly wind; orange: southwesterly wind). Numbered peaks in Figure 1 are emphasized as large crosses, while other marginal peaks are shown by small crosses. Open red and green circles are the locations of offshore platforms in 2010, identified based on DMSP/OLS data and as reported in the EDGAR v.4.2 FT2010 database, respectively. Gray solid lines mark the routes of the VOS ships. The maps used in this figure were generated by Generic Mapping Tools (https://www.soest.hawaii.edu/gmt/).

provided by the US National Oceanic and Atmosphere Administration[15]. Using the nighttime lights data "avg lights x pct", which are annual composite images of noise-filtered nighttime lights data used to infer gas-flaring volumes[16], we identified the locations of offshore platforms within the study area. The distribution of these identified offshore platforms remained largely unchanged throughout our study period. Most of these platforms were either off the east coast of the Malay Peninsula or off the northwest coast of Borneo and were near the locations of the CH$_4$ peaks along the Southeast Asian trade routes (Figure 2). Generally, CH$_4$ is a dominant component of emissions from offshore oil platforms, released as a result of gas flaring and venting, equipment leaks, and evaporation losses, with concomitant emissions of CO$_2$ mainly due to gas flaring[16,17]. These results suggest that the observed CH$_4$ peaks represent emissions from offshore production platforms.

The CH$_4$ emissions from offshore platforms are reported in the anthropogenic trace gas emission inventory database EDGAR (Emission Database for Global Atmospheric Research) v.4.2 FT2010[18]. We compared the distribution of offshore platforms identified in this study to that reported in EDGAR. For the comparison, we used the annual composite image for 2010 from the DMSP/OLS data and annual CH$_4$ emission data for 2010 from EDGAR. This revealed considerable discrepancy in the distribution of offshore platforms, especially off the east coast of the Malay Peninsula, which indicates that the current emission inventories of offshore platforms in Southeast Asia still include considerable uncertainties regarding CH$_4$ and other co-emitted gas components.

Most of our observations were performed during the boreal fall and winter season when strong northeasterly winds associated with the East Asian monsoon prevail off the east coast of the Malay Peninsula; westerly winds passing over the Malay Peninsula from the Indian Ocean prevailed only during September and October of 2009 during our observations. In contrast, there was no prevailing wind direction off the northwest coastal region of Borneo during our study period. Thus, the Malay peaks observed during the northeasterly wind season should represent emissions from offshore platforms windward of the peak locations, whereas the Borneo peaks represent emissions from both offshore platforms and onshore coastal sources. To characterize the offshore platform emissions, we examined the emissions measured during the CH$_4$ peaks based on the CH$_4$–CO$_2$ enhancement ratio ($\Delta CH_4/\Delta CO_2$), which is the linear slope of the correlation of the mole fractions of CH$_4$ and CO$_2$. The observed enhancement ratio can often be used to identify the emission sources because it can be approximated to the emission ratio when observations are performed near the emission sources. For example, past observations at remote sites during wintertime have shown the $\Delta CH_4/\Delta CO_2$ ratios are typically less than about 20 ppb/ppm (ppm is defined as μmol mol^{-1}) in air masses polluted principally by anthropogenic combustion-related emissions in urban and industrialized areas[19–22]. The emission factors of CO$_2$ and CH$_4$ from biomass-burning sources were determined the typical CH$_4$/CO$_2$ ratios to be less than 20 ppb/ppm[23]. These results provide diagnostic criteria for estimating the contributions from these anthropogenic emissions on land.

For further analysis of the $\Delta CH_4/\Delta CO_2$ ratios observed here, we selected 11 distinct Malay peaks and 16 Borneo peaks that showed substantial CH$_4$ increases (>50 ppb) for more than 10 min and significant positive correlations between CH$_4$ and CO$_2$ ($R > 0.4$, p-value < 0.05). The $\Delta CH_4/\Delta CO_2$ ratios during these peaks, calculated by reduced major-axis regression[24], ranged from 8 to 1108 ppb/ppm and from 3 to 880 ppb/ppm for the Malay and Borneo peaks, respectively (Figure 3). The M1, M3, M4, M5, M6, M8, and M9 peaks show similar ΔCO_2-vs.-ΔCH_4 correlative behavior, suggesting that they originated from the same emission process at the offshore platforms. We examined the approximate flaring efficiency (i.e., $\Delta CO_2/(\Delta CO_2 + \Delta CH_4)$ in %) using the ΔCO_2-vs.-$(\Delta CO_2 + \Delta CH_4)$ regression for these peaks. The mean $\Delta CH_4/\Delta CO_2$ ratio for these peaks is 94 ppb/ppm, corresponding to a flaring efficiency of 92%. As gas-flaring efficiencies for industrial flares are usually greater than 90%, it is considered that these plumes originated principally from flaring with the contribution from fugitive emissions (inclusive of venting), if any, being relatively small. The M7, M10, and M11 peaks show higher $\Delta CH_4/\Delta CO_2$ ratios than those of the gas-flaring plumes, suggesting greater contribution from fugitive emissions. These results
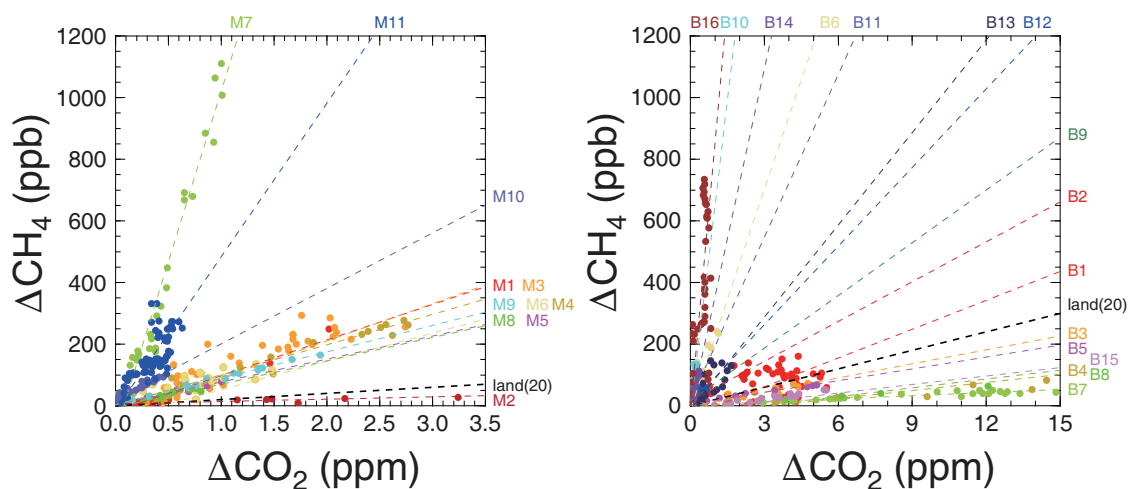
3

Figure 3 | Scatter plots of CH$_4$ versus CO$_2$ mole fractions during observed CH$_4$ peaks. Numbering of peaks is as described in Figure 1. The left and right panels are for the Malay and Borneo peaks, respectively. Dashed lines indicate regression lines for individual peaks determined by reduced major-axis regression. The black dashed line labeled "land(20)" indicates the upper limit of the CH$_4$–CO$_2$ emission ratio for onshore anthropogenic emissions.

indicate that the observed $\Delta CH_4/\Delta CO_2$ ratios can vary widely, depending on the contributions from fugitive emissions. In contrast, the contributions from flaring and fugitive emissions to the M2 peak, associated with the $\Delta CH_4/\Delta CO_2$ ratio of 8 ppb/ppm, appear negligible. Similarly, the 16 peaks observed in the Borneo area with $\Delta CH_4/\Delta CO_2$ ratios higher than 20 ppb/ppm were explained by the mixing of flaring and fugitive emissions. Consequently, we chose those peaks with $\Delta CH_4/\Delta CO_2$ ratios higher than 20 ppb/ppm for further analysis.

Discussion

We used these observed CH$_4$ peaks to estimate the CH$_4$ emission rates based on a mass balance approach[25–27]. Assuming that the CH$_4$ plume was formed steadily during the observation and that the CH$_4$ mixing ratio was vertically well mixed in the MBL, the CH$_4$ emission rate q_{CH4} can be expressed by:

$$q_{CH4} = u \bullet \cos \alpha \bullet n \bullet Z_{MBL} \bullet \int_a^b [f_{CH_4}(y) - C_0(y)] dy \qquad (1)$$

In equation (1), u is the mean horizontal wind speed along the plume axis, α is the angle between the ship transect and the perpendicular to the plume axis, Z_{MBL} is the depth of the MBL, n is the average molar density of air within the MBL, y is the distance from the plume axis, $f_{CH4}(y)$ is the observed CH$_4$ mole fraction at y, and $C_0(y)$ is the background CH$_4$ mole fraction at y. The start and end points of the integration interval for the individual CH$_4$ peaks, a and b in equation (1), are determined manually by visual inspection, and the values of $C_0(y)$ are determined practically by linear interpolation between the CH$_4$ mole fractions at points a and b. As no meteorological observations were performed onboard, the mean wind speeds and directions and the depths of the MBL were estimated based on the CGER/METEX three-dimensional kinematic trajectory model[28]. This trajectory model was driven by six-hourly meteorological input data from the NCEP/NCAR reanalysis, which has a spatial resolution of $2.5° \times 2.5°$. The model calculation was initiated at an altitude of 250 m above sea level at the locations of the CH$_4$ peaks. For every plume calculation, we adopted the molar density of air (n) of 1.2 kg m^{-3}, which was the average value of n at 0 and 0.5 km[29]. We applied the mass balance approach to the appropriate 14 peaks that the ship transited straight across the CH$_4$ peak. Geographical relationships between the observed CH$_4$ peaks and the offshore platforms were well explained by the trajectory model. The resultant CH$_4$ emission

rates for the eight Malay platform peaks: M1, M3, M4, M5, M6, M7, M8, and M9 are within the range of 3.9–426.7 g s^{-1} with a median (mean) of 99.2 (124.7) g s^{-1}. The rates for the six Borneo platform peaks: B1, B6, B11, B12, B13, and B14 are within the range of 1.8–46.0 g s^{-1} with a median (mean) of 14.7 (16.9) g s^{-1}, as summarized in Table 1, together with the values of the parameters used in the calculations. These estimates are comparable with the recent preliminary estimates using the Visible Infrared Imaging Radiometer Suite on board the Suomi National Polar-orbiting Partnership satellite, provided by the National Geophysical Data Center of the National Oceanic and Atmospheric Administration[30]. As conservative error estimates, we evaluated uncertainty ranges for the emission rates by assuming the relative uncertainty of $\pm 50\%$ for the two dominant factors (u $\times$ cosθ and Z$_{MBL}$), and ± 0.05 kg m^{-3} for the molar density of air (1.2 kg m^{-3}). The calculated uncertainty ranges (from lower to upper limits), also listed in Table 1, suggest substantial uncertainty in this approach.

The median value of all the CH$_4$ emission rates is 29.2 g s^{-1}. Using the DMSP satellite, we identified 112 offshore platforms in the Southeast Asian region (defined as: 15°N–10°S, 90°–140°E); thus, the resultant regional total emission rate is calculated as 3.3 kg s^{-1}. The total regional annual emission of CH$_4$ from offshore platforms in the Southeast Asian region is estimated to be about 0.1 Tg y^{-1}, associated with an uncertainty range of 0.02–0.32 Tg y^{-1} (the median values of the lower and upper limits). EDGAR reports that annual CH$_4$ emissions from oil and gas production in 12 Southeast Asian countries (Brunei, Cambodia, Lao, Myanmar, Malaysia, the Philippines, Singapore, Thailand, Timor, Vietnam, Indonesia, and Papua New Guinea) were about 3.7 Tg y^{-1} for 2010, which corresponds to about 1% of the 335 Tg y^{-1} global anthropogenic CH$_4$ emissions[18]. Offshore CH$_4$ emissions account for about 8% (0.29 Tg y^{-1}) of the total emissions from oil and gas production in the Southeast Asian region. Despite the large uncertainty inherent in the mass balance approach, our estimate displays relatively good agreement with that by EDGAR. However, we note substantial differences in the locations of the offshore platforms between the EDGAR inventory and those determined by DMSP satellite observation. The distributions of point sources of CH$_4$ are an important uncertainty in the existing inventories. The relative contributions of the offshore CH$_4$ emissions to the regional CH$_4$ emissions in Southeast Asia are estimated to be about 3% for the oil and gas production sector (both offshore and onshore) (3.7 Tg y^{-1}, as esti-

Table 1 | Estimated CH$_4$ emission rates for the observed CH$_4$ peaks

Area	Peak No.	u (m s^{-1})	α (deg.)	Z_{MBL} (m)	$\int_a^b [f_{CH_4}(y) - C_0(y)]dy$ (ppm m $\times$ 10^4)	q_{CH_4} (g s^{-1})
Malay	M1	2.4	38.0	565	1.4	38.1 (9.1–89.3)
	M3	2.8	2.1	252	10.0	180.8 (43.3–423.8)
	M4	5.0	23.4	430	2.6	133.0 (31.9–311.8)
	M5	5.1	12.2	556	0.23	16.8 (4.0–39.4)
	M6	5.8	25.4	505	1.6	110.7 (26.5–259.5)
	M7	2.1	46.5	574	20.2	426.7 (102.2–1000.0)
	M8	2.2	7.5	607	0.11	3.9 (0.9–9.2)
	M9	2.6	8.9	677	1.9	87.7 (21.0–205.5)
Borneo	B1	3.6	82.1	517	7.0	46.0 (11.0–107.9)
	B6	3.4	9.9	469	0.43	17.5 (4.2–41.1)
	B11	0.8	11.7	651	0.31	4.0 (1.0–9.3)
	B12	3.9	78.9	597	0.16	1.8 (0.4–4.3)
	B13	3.9	78.0	588	1.6	20.2 (4.9–47.5)
	B14	3.0	78.9	674	1.2	11.8 (2.8–27.6)

The value of 1.2 kg m^{-3} is used for the molar density of air to calculate the CH$_4$ emission rates. Figures in parentheses are the uncertainty ranges.

mated by EDGAR), and about 0.2% for the anthropogenic sources (63 Tg y^{-1}, as estimated by EDGAR).

The global CH$_4$ emissions in 2011 are estimated to be 556 ± 56 Tg y^{-1}, with contributions from natural and anthropogenic emissions being comparable[31]. Natural emissions from wetlands are the single most dominant contributor to the total CH$_4$ emissions, with the annual emissions being approximately 200 Tg y^{-1}. The middle-class sources with the annual emissions in the range of 10–100 Tg y^{-1} include fossil fuels, ruminants, landfills/waste, geological sources, freshwater, rice paddies, burning of biomass/biofuels, wild animals, and termites. The emissions from other sources are minor. The emissions (and range) from hydrates, wildfires, and permafrost are estimated to be 6 (2–9), 3 (1–5), and 1 (0–1) Tg y^{-1}, respectively.

Globally, there are a number of offshore fields for oil and gas production. In addition to Southeast Asia, the North Sea, Persian Gulf, Gulf of Guinea, and Gulf of Mexico are known to be active in oil and gas production. As noted above, our estimate and EDGAR are in relatively good agreement for offshore CH$_4$ emissions in Southeast Asia. A simple global estimate based on EDGAR implies that CH$_4$ emissions from worldwide offshore oil and gas platforms are 1–2 Tg y^{-1}, suggesting that the emissions from offshore sources may be comparable to those from minor natural sources such as wildfires and permafrost.

To our knowledge, this work marks the first top-down constraint on CH$_4$ emissions from oil and gas platforms in Southeast Asia. On the other hand, we also realize the considerable uncertainty in our estimates, which derive from a combination of features inherent in the mass balance approach and the lack of samples of CH$_4$ plumes from offshore platforms, due to the sporadic occurrence of gas flaring and fugitive emissions at oil and gas platforms. Hence, our top-down estimates of CH$_4$ emissions from offshore platforms located in the Southeast Asian region need to be tested and improved. For example, if fugitive plumes were undersampled in our observations, the estimated CH$_4$ emissions would be much greater, possibly even by one order of magnitude. To better assess the regional total emissions of CH$_4$ from offshore platforms and thereby improve the current emissions inventory, further top-down constraints by integrated ship, aircraft, and satellite observations are needed. In particular, the detection of fugitive plumes would be useful to reduce uncertainties in estimating the emissions. Current estimates of CH$_4$ emissions from oil and gas processes were approximately 20% of worldwide anthropogenic emissions in 2010, and they are expected to increase by nearly 35% between 2010 and 2020[32]. The feedback gained from plume observations can help in the reduction of fugitive emissions in

Southeast Asian countries and thus, contribute to the mitigation of global warming.

Methods

We used two commercial cargo vessels in the VOS program in Southeast Asia: the M/V *Fujitrans World* (owned by the Kagoshima Senpaku Kaisya, Ltd., Japan) was the primary vessel with backup provided by the M/V *Trans Future 1* (owned by the Toyofuji Shipping Co. Ltd., Japan). These ships regularly sail the trade routes between Japan and Southeast Asia, berthing at Osaka, Yokohama, and Nagoya (Japan); Hong Kong (China); Laem Chabang (Thailand); Singapore; Port Klang, Kuching and Kota Kinabalu (Malaysia); Jakarta (Indonesia); and Muara (Brunei) at four-week intervals (Figure 4). Two northbound routes are used from Jakarta to Japan: one via Thailand and the Philippines (the northbound Asia route) and the other via Borneo (the northbound Borneo route). Only one southbound route is used from Japan to Indonesia.

Onboard each VOS ship, continuous measurements of CO$_2$, CO, and O$_3$ were performed using a non-dispersive infrared analyzer (NDIR), an NDIR with gas filter correlation, and an ultraviolet absorption analyzer, respectively. The continuous CO$_2$ data processed for public use are available at our webpage (http://soop.jp/). Flask samples were also collected for laboratory analysis of CO$_2$, CO, CH$_4$, N$_2$O, SF$_6$, H$_2$,
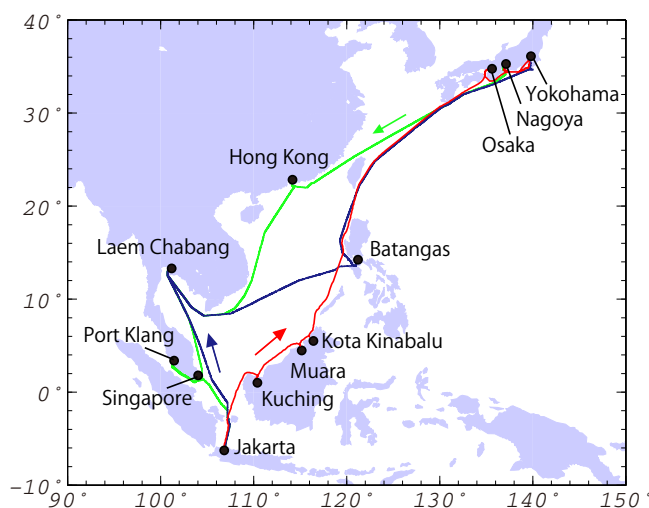

Figure 4 | The VOS shipping routes in Southeast Asia. Green and blue lines show the southbound (Japan–Indonesia) and northbound (Indonesia–Japan) Asia routes respectively; a red line shows the northbound Borneo route (Indonesia–Japan). Regular berthing ports are shown as solid black circles. The maps used in this figure were generated by Generic Mapping Tools (https://www.soest.hawaii.edu/gmt/).

O_2/N_2, and CO_2 isotopologues ($^{13}CO_2$, $^{12}C^{18}O^{16}O$). A detailed description of the atmospheric observation system is provided elsewhere[13].

In September 2009, continuous measurements of atmospheric CO_2 and CH_4 were commenced on VOS ships along both of the Southeast Asian routes using wavelength-scanned cavity ring-down spectroscopy (WS-CRDS) instruments (Picarro Inc., Santa Clara, CA, USA, models EnviroSense 3000i and G1301). Air sample was collected from the air intake set at the top deck of the ship (approximately 50 m above sea level) using a diaphragm pump placed in the observation room. The sampled air was dried before analysis to minimize biases due to dilution and pressure-broadening effects of water vapor on the WS-CRDS measurements. The sampled air was dehumidified by passing it through a sample-drying unit consisting of an electric cooler kept at $+1°C$ and a Nafion Perma Pure dryer (Perma Pure LLC, Toms River, NJ, USA). The design and performance of the unit was very similar to that used for the CO measurements[13]. The sampled air was dried to less than ~0.3% water (as measured by the WS-CRDS) before the mole fractions of CO_2 and CH_4 were determined based on the water vapor content according to an instrument-specific water vapor collection function[33]. To our experience, the air samples were rarely contaminated with the ship's exhaust, when the ship sails at approximately 20 knot because the ship's exhaust is located at stern side. When the air samples were contaminated with the exhaust gas, we judged it by the CO_2 and O_3 measurements (CO_2 increase and O_3 decrease), and then rejected the data before the analysis.

For instrument calibration, we prepared a set of three natural or purified air-balanced standard gases with CO_2 and CH_4 (ca. 380, 400, and 420 ppm for CO_2, and 1800, 2000, and 2200 ppb for CH_4) in our laboratory to prevent pressure-broadening effects due to the different air compositions of the samples and standard gases. The standard gases were introduced into the WS-CRDS instrument daily in series, 10 min for each gas. The mole fractions of CO_2 and CH_4 in the standard gases were calibrated against NIES standard gas scales (NIES 09 for CO_2, NIES 96 for CH_4), which are traceable to World Meteorological Organization standard gas scales. The analytical precision for 1-min measurements by the WS-CRDS instruments of CO_2 and CH_4 were typically 0.05 ppm and 0.5 ppb (1 sigma), respectively. In this study, we used only the 1-min temporal mean CH_4 data from the continuous measurements because of the coarse resolution of the CO data, available only as 1-hour means from the gas filter correlation measurements, and because the O_3 data provide little information about CH_4 emission sources.

1. Fiore, A. M. et al. Linking ozone pollution and climate change: The case for controlling methane. Geophys. Res. Lett. **29**, 1919, doi:10.1029/2002GL015601 (2002).

2. Prather, M. J., Holmes, C. D. & Hsu, J. Reactive greenhouse gas scenarios: Systematic exploration of uncertainties and the role of atmospheric chemistry. Geophys. Res. Lett. **39**, L09803, doi:10.1029/2012GL051440 (2012).

3. Montzka, S. A., Dlugokencky, E. J. & Butler, J. H. Non–CO₂ greenhouse gases and climate change. Nature **476**, 43–50, doi:10.1038/nature10322 (2011).

4. Shindell, D. et al. Simultaneously mitigating near-term climate change and improving human health and food security. Science **335**, 183–189, doi:10.1126/science.1210026 (2012).

5. Dlugokencky, E. J. et al. Observational constraints on recent increases in the atmospheric CH₄ burden. Geophys. Res. Lett. **36**, L18803, doi:10.1029/2009GL039780 (2009).

6. Aydin, M. et al. Recent decreases in fossil–fuel emissions of ethane and methane derived from firn air. Nature **476**, 198–201 (2011).

7. Kai, F. M., Tyler, S. C., Randerson, J. T. & Blake, D. R. Reduced methane growth rate explained by decreased Northern Hemisphere microbial sources. Nature **476**, 194–197, doi:10.1038/nature10259 (2011).

8. Levin, I. et al. No inter–hemispheric δ¹³CH₄ trend observed. Nature **486**, E3–E4, doi:10.1038/nature11175 (2012).

9. Simpson, I. J. et al. Long–term decline of global atmospheric ethane concentrations and implications for methane. Nature **488**, 490–494, doi:10.1038/nature11342 (2012).

10. Frankenberg, C. et al. Global column–averaged methane mixing ratios from 2003 to 2009 as derived from SCIAMACHY: Trends and variability. J. Geophys. Res. **116**, doi:10.1029/2010JD014849 (2011).

11. Beck, V. et al. Methane airborne measurements and comparison to global models during BARCA. J. Geophys. Res. **117**, D15310, doi:10.1029/2011JD017345 (2012).

12. Baker, A. K. et al. Estimating the contribution of monsoon-related biogenic production to methane emissions from South Asia using CARIBIC observations. Geophys. Res. Let. **39**, L10813, doi:10.1029/2012GL051756 (2012).

13. Nara, H. et al. Onboard measurement system of atmospheric carbon monoxide in the Pacific by voluntary observing ships. Atmos. Meas. Tech. **4**, 2495–2507, doi:10.5194/amt-4-2495-2011 (2011).

14. Terao, Y. et al. Interannual variability and trends in atmospheric methane over the western Pacific from 1994 to 2010. J. Geophys. Res. **116**, D14303, doi:10.1029/2010JD015467 (2011).

15. National Geophysical Data Center. Version 4 DMSP-OLS Nighttime Lights Time Series. http://ngdc.noaa.gov/eog/dmsp/downloadV4composites.html (2013) (Date of access: 05/04/2014).

16. Elvidge, C. D. et al. A fifteen year record of global natural gas flaring derived from satellite data. Energies **2**, 595–622, doi:10.3390/en20300595 (2009).

17. Howarth, R. W., Santoro, R. & Ingraffea, A. Methane and the greenhouse-gas footprint of natural gas from shale formations. Clim. Change **106**, 679–690 (2011).

18. European Commission – JRC Joint Research Centre and PBL Netherlands Environmental Assessment Agency. EDGAR - Emission Database for Global Atmospheric Research, v4.2 FT2010. http://edgar.jrc.ec.europa.eu (2013) (Date of access: 22/05/2014).

19. Conway, T. J. & Steele, L. P. Carbon dioxide and methane in the Arctic atmosphere. J. Atmos. Chem. **9**, 81–99 (1989).

20. Schmidt, M., Graul, R., Sartorius, H. & Levin, I. Carbon dioxide and methane in continental Europe: a climatology, and ²²²Radon–based emission estimates. Tellus **48B**, 457–473 (1996).

21. Necki, J. et al. Six-year record of atmospheric carbon dioxide and methane at a high-altitude mountain site in Poland. Tellus **55B**, 94–104 (2003).

22. Tohjima, Y. et al. Temporal changes in the emissions of CH₄ and CO from China estimated from CH₄/CO₂ and CO/CO₂ correlations observed at Hateruma Island. Atmos. Chem. Phys. **13**, 22893–22930, doi:10.5194/acpd-13-22893-2013 (2013).

23. Akagi, S. K. et al. Emission factors for open and domestic biomass burning for use in atmospheric models. Atmos. Chem. Phys. **11**, 4039–4072, doi:10.5194/acp-11-4039-2011 (2011).

24. Ayers, G. P. Comment on regression analysis of air quality data. Atmos. Environ. **35**, 2423–2425 (2001).

25. Ryerson, T. B. et al. Emissions lifetimes and ozone formation in power plant plumes. J. Geophys. Res. **103**, 22569–22583 (1998).

26. Turnbull, J. C. et al. Assessment of fossil fuel carbon dioxide and other anthropogenic trace gas emissions from airborne measurements over Sacramento, California in spring 2009. Atmos. Chem. Phys. **11**, 705–721, doi:10.5194/acp–11–705–2011 (2011).

27. Karion, A. et al. Methane emissions estimate from airborne measurements over a western United States natural gas field. Geophys. Res. Lett. **20**, 703–706, doi:10.1029/93GL00753 (2013).

28. Zeng, J. et al. A study of trajectory quality using methane measurements from Hateruma Island. Atmos. Environ. **37**, 1911–1919 (2003).

29. National Oceanic and Atmospheric Administration, National Aeronautics and Space Administration, and United States Air Force. U.S. Standard Atmosphere, 1976. US Government Printing Office, Washington, D.C. (1976).

30. National Geophysical Data Center. VIIRS Nightfire, Nighttime Detection and Characterization of Combustion Sources. http://ngdc.noaa.gov/eog/viirs/download_viirs_fire.html (2013) (Date of access: 05/04/2014).

31. Intergovernmental Panel on Climate Change (IPCC). Climate Change 2013: The Physical Science Basis. Contribution of Working Group I to the Fifth Assessment Report of the Intergovernmental Panel on Climate Change, edited by Stocker et al., 1535 pp., Cambridge University Press, Cambridge, United Kingdom and New York, NY, USA, doi:10.1017/CBO9781107415324 (2013).

32. Global Methane Initiative. Oil and gas systems. https://www.globalmethane.org/oil-gas/index.aspx (2004) (Date of access: 05/04/2014).

33. Nara, H. et al. Effect of air composition (N₂, O₂, Ar, and H₂O) on CO₂ and CH₄ measurement by wavelength-scanned cavity ring-down spectroscopy: calibration and measurement strategy. Atmos. Meas. Tech. **5**, 2689–2701, doi:10.5194/amt-5-2689-2012 (2012).

Author contributions

H.N. and H.T. took the main role in the study design and the data analyses. Y.T. actively participated in the analyses and discussion, H.M. and Y.N. took the leading role in the operation of the monitoring project, T.M. took the key role in the assurance of data quality. All authors participated in the discussion of results and H.N., H.T. and Y.T. wrote the manuscript.

Additional information

Competing financial interests: The authors declare no competing financial interests.

How to cite this article: Nara, H. et al. Emissions of methane from offshore oil and gas platforms in Southeast Asia. Sci. Rep. **4**, 6503; DOI:10.1038/srep06503 (2014).